Earthquakes and Structures, *Vol. 16, No. 5 (2019) 533-546*
DOI: https://doi.org/10.12989/eas.2019.16.5.533

Cyclic performance of steel fiber-reinforced concrete exterior beam-column joints

Romanbabu M. Oinam[1a], P.C. Ashwin Kumar[2b] and Dipti R. Sahoo[*3]

[1]Department of Civil and Environmental Engineering, Indian Institute of Technology Tirupati, Tirupati-517506, India
[2]Department of Earthquake Engineering, Indian Institute of Technology Roorkee, Roorkee 247667, India
[3]Department of Civil Engineering, Indian Institute of Technology Delhi, New Delhi-110016, India

(Received February 1, 2019, Revised March 25, 2019, Accepted March 26, 2019)

Abstract. This study presents an experimental investigation on six beam-column joint specimens under the lateral cyclic loading. The aim was to explore the effectiveness of steel fiber-reinforced concrete (SFRC) in reducing the transverse shear stirrups in beam-column joints of the reinforced concrete (RC) frames with strong-columns and weak-beams. Two RC and four SFRC specimens with different types of reinforcement detailing and steel fibers of volume fraction in the range of 0.75-1.5% were tested under gradually increasing cyclic displacements. The main parameters investigated were lateral load-resisting capacity, hysteresis response, energy dissipation capacity, stiffness degradation, viscous damping variation, and mode of failure. Test results showed that the diagonally bent configuration of beam longitudinal bars in the beam-column joints resulted in the shear failure at the joint region against the flexural failure of beams having straight bar configurations. However, all SFRC specimens exhibited similar lateral strength, energy dissipation potential and mode of failure even in the absence of transverse steel in the beam-column joints. Finally, a methodology has been proposed to compute the shear strength of SFRC beam-column joints under the lateral loading condition.

Keywords: beam-column joints; cyclic loading; failure; reinforcement detailing; steel fiber-reinforced concrete

1. Introduction

Reinforced concrete (RC) structural systems should have adequate lateral strength, lateral stiffness, and displacement ductility to resist the earthquake-induced demands without collapse (Paulay and Priestley 1992). Displacement ductility of a RC frame primarily depends on the inelastic rotational capacity of beams and columns. Strong column-weak beam (SC-WB) philosophy is widely adopted in the earthquake-resistant design to ensure a ductile mode of failure in the extreme events. This requires that the inelastic rotation or formation of plastic hinges should occur only in beams only with limited yielding at the column bases. Thus, beam-column joints in a RC frame should enable the adjoining beams and columns to develop their maximum strengths and deformation capacities. Under the action of lateral loading, these beam-column joints are subjected to high shear force demand and their seismic performance is often limited by the bond and shear failure mechanisms (Park and Paulay 1975). This does not ensure adequate structural ductility if not properly accounted through design and detailing (Harajli *et al.* 1995, Murty *et al.* 2003).

Extensive studies have already been conducted to investigate the load-resisting mechanism of RC beam-column joints under lateral loading condition. Paulay *et al.* (1978) proposed a shear-resisting mechanism in RC beam-column joints under reversed cyclic loading considering the contribution of joint shear reinforcement and the concrete strut. Park and Mosalam (2012) developed a shear strength model and a moment-rotation relationship for unreinforced corner beam-column joint. The findings of these studies have been considered in developing the design guidelines and reinforcement detailing of RC beam-column joints in many building codes (e.g., IS:1893 2016, ASCE 41-13 2013, Eurocode 8 2004). However, these provisions may result in the considerable amount of reinforcement leading to the difficulty in concrete placement in the beam-column joint regions. Further, past experimental studies (e.g., Tsonos *et al.* 1992, Tsonos 2007) have concluded that the beam-column joints having conventional reinforcement detailing may suffer from excessive damage under seismic loading. These joints may not able to resist the shear stresses higher than those recommend by the design codes. The increase in flexural strengths of columns as compared to beams may not be adequate to avoid the early shear failure of these joints.

Various techniques have been studied in the past in order to improve the seismic performance of RC beam-column joints. These techniques include the use of additional reinforcing steel (Chutarat and Aboutaha 2003, Lu *et al.* 2012), headed or hooked bars (Rajagopal *et al.* 2014), ferro-cement jackets (Li *et al.* 2015), prestressed steel strips

*Corresponding author, Associate Professor
E-mail: drsahoo@civil.iitd.ac.in
[a]Assistant Professor
E-mail: romanbabu@iittp.ac.in
[b]Assistant Professor
E-mail: pcashwin.feq2018@iitr.ac.in

ISSN: 2092-7614 (Print), 2092-7622 (Online)

(Yang *et al.* 2018), and C-FRP sheets (Karayannis and Golias 2018). Tsonos *et al.* (1992) studied the efficiency of non-conventional reinforcement detailing by using crossed inclined bars in the exterior beam-column joints. The presence of inclined bars not only controlled the occurrence of diagonal brittle shear failure of the exterior beam-column joints, but also helped in maintaining the load-resisting capacity of joints for a higher level of displacement ductility. In addition, these inclined bars in the joint regions were found to be effective in controlling the second-order effects and the axial load variations in the structrual elements (Tsonos *et al*. 2004). Steel fiber-reinforced concrete (SFRC) is used as one of the alternatives to reduce the reinforcement congestion while maintaining the similar strength and the better ductility and energy dissipation at a lesser cost (Liu 2006, Oinam *et al*. 2014). The volume fraction, aspect ratio, bond characteristics, and surface deformation characteristics of steel fibers strongly influence the load-resisting capacity, displacement ductility, mode of failure, and flexural toughness of SFRC beams (e.g., Lee 2007, Dinh *et al.* 2010, Aoude *et al*. 2012, Sahoo and Sharma 2014, Sahoo and Kumar 2015, Sahoo *et al.* 2015). SFRC beam-column joints have shown the improved load-resisting capacity, displacement ductility, and energy dissipation under cyclic loading as compared to the conventional RC joints (Bayasi and Gebman 2002, Abbas *et al.* 2014, Kheni *et al.* 2015). SFRC directly engages with the bond and shear mechanism of the joint, thereby, providing the better damage tolerance. Steel fiber-reinforced high-strength or ultra high-strength concrete jackets have found to be very effective in improving the seismic performance of the deficient beam-column joints (Tsonos 2014).

The present study is focused on the evaluation of the cyclic behavior of exterior beam-column joints reinforced with crossed inclined bars and SFRC. The longitudinal reinforcement bars of beams were bent in to the joints unlike the column reinforcing steel as studied by Tsonos *et al.* (1992). An experimental investigation has been conducted to compare the cyclic response of conventionally reinforced exterior beam-column joints with those of SFRC specimens. The main parameters varied in this study are the volume fraction of steel fibers in concrete and the detailing of reinforcing steel in the beam-column joints. The aim is to achieve a preferred mode of failure, i.e., plastic hinging in beams by delaying the failure of beam-column joints under cyclic loading.

2. Research signifcance

Extensive studies in past five decades have been conducted on beam-column joints considering different arrangements of reinforcement bars and types of fiber-reinforced concrete. These studies have highlighted the improved overall behavior of beam-column joints under different loading conditions. In many cases, the reduction in transverse steel in the beam-column joints has resulted in the shear failure at the beam-column interfaces. The beam-column joints with SFRC and vertical column reinforcement bars in the joint regions have not performed well in the past studies (e.g., Tsonos *et al.* 1992). Hence, there is a need for a further study on SFRC beam-column joints having various reinforcement detailing schemes and geometric parameters. In this study, six exterior beam-column joints with plain concrete as well as SFRC were tested under cyclic loading until their failure. The influence of different detailing schemes, column and beam dimensions, percentage of steel, column shear span, and fiber volume fraction on the overall joint behavior was investigated. A methodology has been proposed to evaluate the contribution of SFRC in the lateral load resistance of beam-column joints under the lateral loading condition.

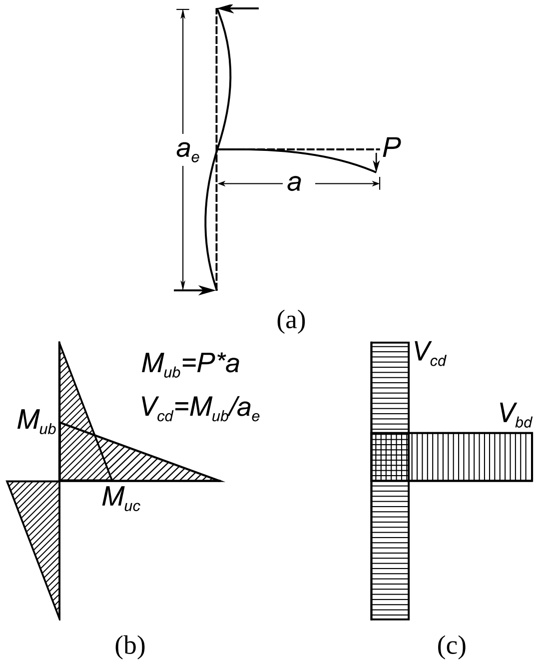

Fig. 1 (a) Displacement response, (b) Bending moment diagram and (c) Shear force diagram of exterior beam-column joint sub-assemblage

3. Experimental investigation

Fig. 1 shows a typical exterior beam-column joint between the point of inflections in columns and beam of a RC frame. For a frame under the action of combined gravity and lateral loadings, the beam-column joint region is subjected to the high bending moment, shear and axial forces. This type of beam-column joint has been considered in the experimental study. The details of test specimens, materials used, test set-up, loading history, and instrumentation are discussed in the following sections.

3.1 Test specimens

Six test specimens representing the exterior beam-column joint of a RC moment-resisting frame were selected for the experimental investigations. Exterior beam-column joints were selected as they represent the highly-stressed condition in comparison to the interior beam-column joints under seismic loading (Barbhuiya and Choudhury 2015).

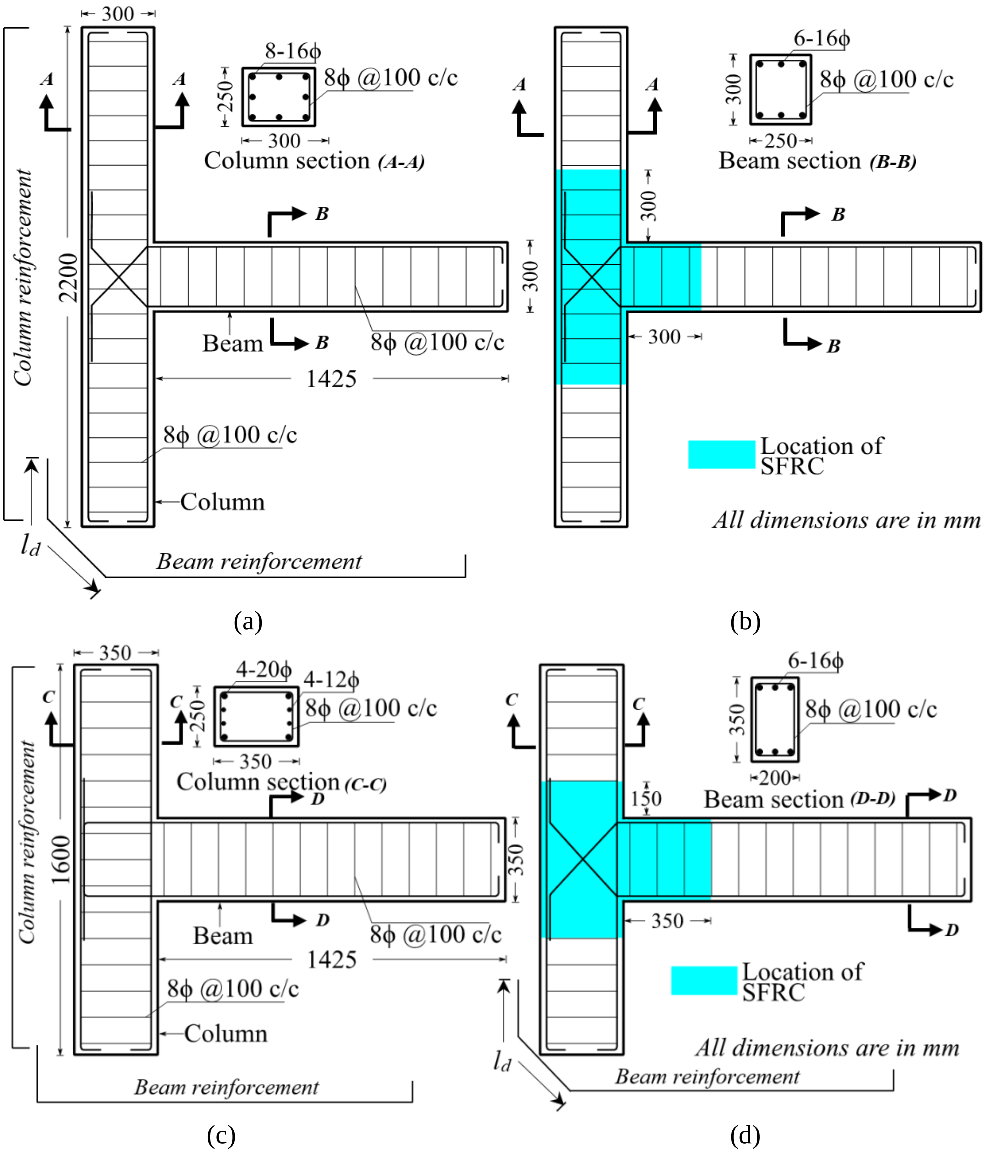

Fig. 2 Details of test specimens (a) RC-1, (b) SFRC-0.75% and SFRC-1.0%(1), (c) RC-2, (d) SFRC-1.0%(2) and SFRC-1.5%

Two specimens represented the conventionally reinforced specimens (i.e., RC-1 and RC-2) without any fiber-reinforced concrete. Other four test specimens (i.e., SFRC-0.75%, SFRC-1.0%(1), SFRC-1.0%(2), and SFRC-1.5%) had SFRC of fiber content of 0.75, 1.0 and 1.50% used in the critical joint regions. Fig. 2 shows the geometric dimensions and reinforcement detailing of all test specimens. Cover concrete used in column and beam were 40 mm and 25 mm, respectively. The shaded regions in Fig. 2 represent the regions where SFRC was used. The reinforcement detailing in beams and columns of the control specimens (RC-1 and RC-2) was carried out in accordance with Indian Standard IS: 456 (2000) provisions without considering the ductile detailing requirements (e.g., without any confining reinforcements at the plastic hinge regions). Table 1 summarizes the effective lengths of members, percentage of longitudinal steel in beam and columns, and the spread of SFRC in beams and columns. In addition to the variation in column and beam cross-section and reinforcing steel, shear span (a) to effective depth (d) ratio

Table 1 Dimensions and reinforcement detailing of the specimens

Specimen	Beam			Column			Fibre content (%)
	l_b, mm	ρ_t (%)	ρ_b (%)	l_c, mm	ρ (%)	L/d	
RC-1	1275	0.95	0.95	2050	2.6	8.4	0
RC-2	1275	0.95	0.95	1450	2.4	4.9	0
SFRC-0.75%	1275	0.95	0.95	2050	2.6	8.4	0.75
SFRC-1.0%(1)	1275	0.95	0.95	2050	2.6	8.4	1.0
SFRC-1.0%(2)	1275	0.95	0.95	1450	2.4	4.9	1.0
SFRC-1.5%	1275	0.95	0.95	1450	2.4	4.9	1.5

of columns were varied maintaining the constant values of a/d ratio for all beams.

As shown in Fig. 2, different reinforcement detailing schemes were adopted in the beam-column joints of test specimens. Test specimens RC-1, SFRC-0.75%, and SFRC-1.0%(1) had same column and beam sections as well as

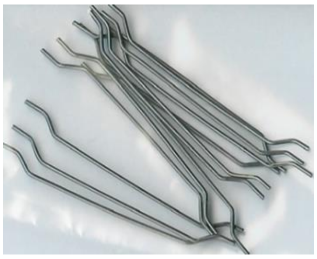

(a)

(b)

Fig. 3 (a) End-hooked type steel fibers and (b) steel fiber reinforced concrete matrix

reinforcement detailing. Eight nos. of 16 mm diameter bars were used as longitudinal steel in column. Similarly, test specimens RC-2, SFRC-1.0%(2) and SFRC-1.5% had the same dimensions and reinforcing steel. Columns of these specimens had four nos. of 20 mm steel bars at corners and four nos. of 12 mm diameter bars. Six nos. of 16 mm diameter bars were used as longitudinal steel in beams of all test specimens. All longitudinal reinforcement bars in columns were kept in the straight configuration in all test specimens. Except the specimen RC-2, all longitudinal bars of beams were bent in the opposite diagonal directions at angle of 45° traversing the beam-column joint core concrete. 8 mm diameter bars at a spacing of 100 mm on centers were used as transverse reinforcing steel in the members and within the joint regions, wherever applicable. Similar detailing of beam longitudinal bars was adopted in the specimens SFRC-1.0%(2), and SFRC-1.5% except that no transverse stirrups were not used within the beam-column joint regions. It was expected that the enhanced shear strength of SFRC should be adequate to resist the shear demand along with the dowel action of the main longitudinal bars.

3.2 Material properties

Ordinary Portland Cement (OPC) of grade 43 and natural sand conforming to Zone II (IS:10262 2009) as the fine aggregates were used in cement concrete for the preparation of test specimens. The maximum size of the coarse aggregate was limited to 20 mm. The design mix proportion for plain concrete with water-cement ratio of 0.43 was set as 1:1.77:3.16 (cement sand: coarse aggregate). Glenium plasticizer of 0.8% of cement weight was used to increase the workability of the fresh concrete. End-hooked type of steel fiber of 60 mm long and 1.0 mm diameter (i.e., fiber aspect ratio=60) was used in the preparation of SFRC. The specified tensile yield strength of steel fibers was 1100 MPa. A higher quantity of plasticizer (1%) was used in SFRC as the inclusion of steel fibers would reduce the workability of fresh concrete. Fig. 3 shows the end-hooked steel fibers and state of fresh SFRC.

Material testing was conducted to determine the actual compressive and tensile properties of plan and fiber-reinforced concrete. Both cube and cylinder compressive strengths of concrete were determined in accordance with Indian Standard IS:516-1959 (2004) guidelines. Table 2 summarizes the mean values of 28-days compressive strengths of plain and fiber reinforced concrete. No significant difference in the compressive strength was noted between the plain concrete and SFRC. SFRC exhibited marginally (<5%) higher compressive strengths as compared to the plain concrete. Thermo-mechanically treated (TMT) steel reinforcement bars were used as both the longitudinal reinforcement and transverse stirrups in the test specimens. Coupon test results showed that the mean values of yield strength, ultimate tensile strength and percentage elongation of reinforcement bars were 415 MPa, 485 MPa and 14.5%, respectively. Table 2 also summarizes the average values of split-tension strength of plain and fiber-reinforced concrete (IS:5816 1999). The increase in split-tension strength of SFRC was in the range of 40-80% as compared to the plain concrete with fiber volume fraction of 0.75-1.5%. Similarly, the flexural tension test conducted on the small-scale beams of size 100 mmx100 mmx500 mm in accordance with ASTM C1609 (2006) guidelines exhibited the enhanced the flexural tensile strength of SFRC in the range of 35-50% as compared to those for the plain concrete (Table 2).

Table 2 Material properties of plain and steel fiber-reinforced concrete

Specimen	Cube compressive Strength, MPa	Cylinder compressive strength, MPa	Split-tensile strength, MPa	Flexural tensile strength, MPa
RC-1	51.7	38.6	3.5	15.5
SFRC-0.75%	52.8	44.0	5.4	21.0
SFRC-1.0%(1)	54.7	42.4	6.7	23.5
RC-2	52.9	41.5	4.1	16.0
SFRC-1.0%(2)	53.8	43.0	5.7	21.5
SFRC-1.5%	55.5	44.8	7.0	24.5

3.3 Test set-up

Test specimens were casted in the horizontal position in order to facilitate the proper compaction of fresh concrete in the members and beam-column joints. Test specimens were cured for 28-days under normal water curing condition. Fig. 4 shows the schematic representation of test set-up used in the cyclic testing of specimens. Test specimens were tested with the column in the horizontal and the beam in the vertical positions. A servo-hydraulic actuator of 250 kN force-capacity and 125 mm stroke length was used to apply the reversed cyclic displacements at the free end of beam. The other end of actuator was connected to a strong vertical reaction frame. Three rollers were placed on three sides of the column ends to allow the rotation at these points. In order to restrain the vertical movements, these ends were anchored to the laboratory strong floor. This set-up may not truly represent the point of contraflexure in columns as the anchoring system may offer some resistance to the bending moment developed at these points. In practice, columns of a RC frame carry axial loads under the combined gravity and seismic load effects. Hence, a hydraulic jack was used at one end of the column to apply a constant axial load of 10%

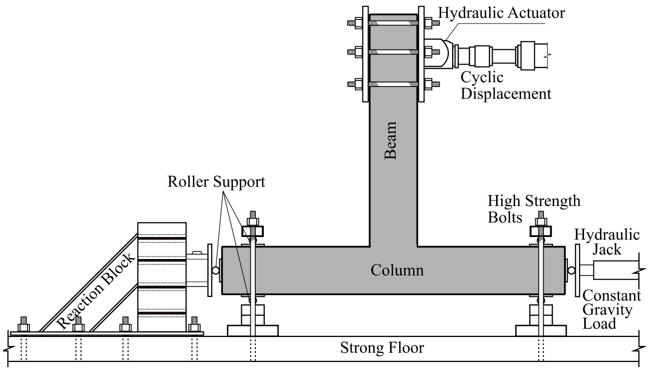

Fig. 4 Test set-up used for cyclic testing of specimens

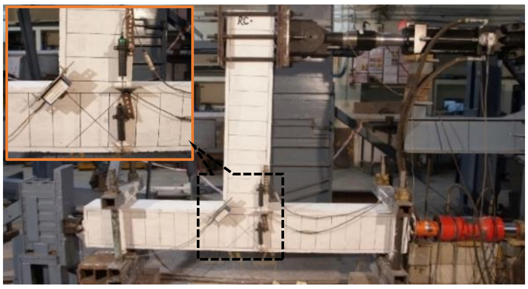

(a)

(b)

Fig. 5 Test specimens (a) RC-1, SFRC-0.75%, SFRC-1.0%(1); (b) RC-2, SFRC-1.0%(2), SFRC-1.5%

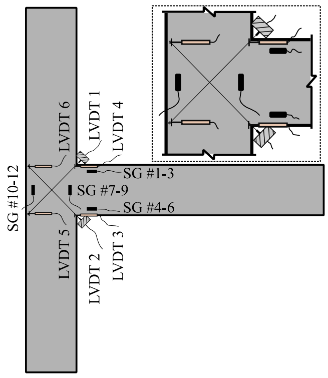

(a)

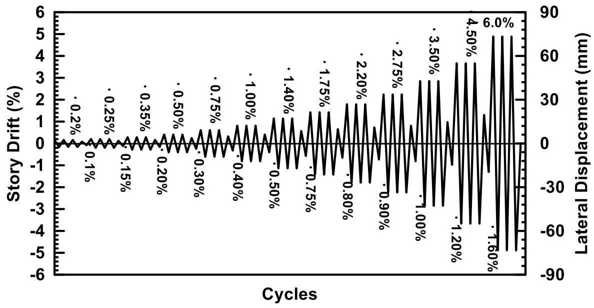

(b)

Fig. 6 (a) Position of strain gauges and displacement sensors in specimen, (b) Displacement history

of the column capacity (Fig. 5). A reaction block was provided at the other end to provide reaction to the applied axial force on the column.

Load cell and displacement sensor of the servo-hydraulic actuator were used to monitor the lateral resistance and displacement of the specimen. Twelve uniaxial electrical-resistance strain gauges (SGs) were attached to the longitudinal bars of columns and beams of specimens to monitor their state of strain under cyclic loading conditions. Fig. 6(a) shows the locations of the strain gauges in the test specimen. Strain gauges attached to column bars were located in the core area of beam-column joints, whereas those on beam bars were placed close to the face of beam-column joint regions. Additionally, four numbers of linear varying differential transformer (LVDTs) and two numbers of string-pot displacement sensors were installed to measure the deformations of beam-column joints in the horizontal and diagonal directions.

Displacement-controlled slow-cyclic testing was conducted on the test specimens to investigate their overall cyclic performance. The imposed displacement history conforms to the recommendation of ACI Committee 374.1-05 (2006) for the slow-cyclic testing of RC specimens. Fig. 6(b) shows the imposed displacement history used in this study. The displacement history consisted of gradually increasing drift ratio cycles of 0.20%, 0.35%, 0.50%, 0.75%, 1.10%, 1.40%, 1.75%, 2.20%, 2.75%, 3.50%, and 4.50%. Drift ratio (or story drift) may be defined as the ratio of the lateral beam displacement to the beam length measured from the column centerline. Each drift cycle was repeated for three times followed by a single drift value of a smaller magnitude. The rate of loading was in the range of 2-5 mm/s. Though it is recommended to carry out the qualifying test on RC components for 3.5% drift ratio (ACI 374.1-05 2006), the specimens were tested till their failure which was much higher than this value. As mentioned earlier, a constant axial load of 10% of column capacity was applied to the column throughout the test. It is worth mentioning that the applied axial load did not truly represent the practical condition but helped in providing necessary axial stability to the test specimen to some extent.

4. Test results

The main parameters investigated in this study were overall behavior, hysteretic response, energy dissipation, state of strain, and mode of failure of test specimens under the slow-cyclic loading in the following sections:

4.1 Overall behavior and mode of failure

Fig. 7 shows the cracks observed in the test specimens

Fig. 7 Location of damages at the failure stage of specimens

and their mode of failure. First visible minor flexural cracks in the beam were first noted in the specimen RC-1 near the beam-column interface at 0.35% drift ratio. First minor diagonal (shear) crack appeared in column of the specimen RC-1 at 0.5% drift. More number of cracks were noted in the beam away from the beam-column joints as the drift magnitude was increased. At 1.4% drift ratio, the maximum width of the crack was measured as 2 mm. At 2.2% drift, the diagonal shear cracks in column extended to more than half of the column depth. The primary mode of failure of the specimen RC-1 was due to the formation of a major crack of 20 mm width at 3.5% drift level. The test was stopped at 4.5% drift because of complete crushing of concrete in the joint region. For the specimen SFRC-0.75% the first crack was noticed at the interface of beam-column at a drift ratio of 0.2%. The crack propagation in specimen SFRC-0.75% was nearly similar to that of the specimen RC-1. The increase in the magnitude of displacement excursion increased the crack width at the beam-column interface of the specimen SFRC-0.75%. The specimen sustained a maximum lateral drift of 4.5%.

All SFRC specimens exhibited the similar behavior with or without transverse steel in the columns at the beam-column joints. Specimen RC-2 exhibited the flexural failure away from the face of beam-column joint along with diagonal cracks in the beam-column joint regions. As expected, more cracks were noted in the beam as compared to the columns because of the smaller flexural capacity of beams. Fig. 8 shows the close-up pictures of mode of failure of test specimens. Test specimens with beam longitudinal bars placed diagonally in the beam-column joints exhibited the interfacial shear cracks irrespective of the quantity of transverse stirrups in the joints. RC specimen with straight beam longitudinal bars exhibited the flexural plastic hinge away from the joint regions.

4.2 Hysteretic response

Fig. 9 shows the lateral force-beam displacement (hysteretic) response of test specimens. As expected, the degradation in strength and stiffness as well as the pinching effect was noted in the cyclic behavior of all test specimens. A higher degradation in post-peak stiffness was noted for SFRC specimens as compared to the RC specimens. Specimen RC-2 exhibited relatively more stable hysteretic response with minor pinching and strength degradation. For the specimen RC-1, the peak values of lateral force of 64.2 and -65.4 kN were noted at 1.4% drift ratio. The

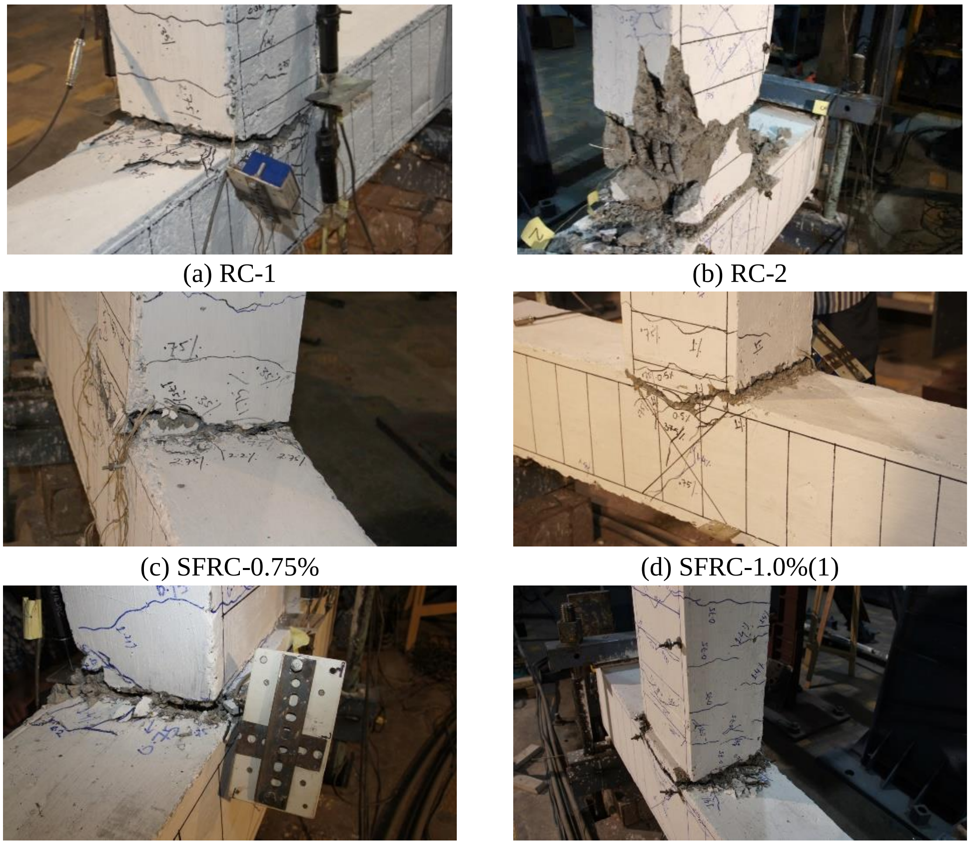

(a) RC-1 (b) RC-2

(c) SFRC-0.75% (d) SFRC-1.0%(1)

(e) SFRC-1.0%(2) (f) SFRC-1.5%

Fig. 8 Close-up pictures showing the mode of failure of test specimens

corresponding values for the specimen RC-2 were 75.7 and -78.6 kN at the same drift level. The higher value of strength for specimen RC-2 can be attributed to the larger cross-section of the beam in comparison to the specimen RC-1 and the difference in the arrangement of the main longitudinal reinforcement in the beam-column joint. Similarly, the specimen SFRC-0.75% exhibited the peak lateral strength of 61.5 and -63.4 kN in the push and pull direction at 1.75% and 1.4% drift ratios, respectively. The corresponding values for the specimen SFRC-1.0%(1) were 59.0 and -55.0 kN at 1.4% drift. For SFRC-1.0%(2), the peak strengths in push and pull direction were observed as 65.7 and -70.9 kN at 1.4% drift. For the specimen SFRC-1.5%, the peak value of strength in the push and pull direction of 1.4% drift level were 65.4 and -72.9 kN, respectively.

A comparison of the backbone curves of the hysteretic response of test specimens is shown in Fig. 10(a). Specimen RC-2 exhibited the higher lateral strength with negligible reduction in the post-peak strength. All other specimens showed the mild reduction in the post-peak strength. SFRC specimens without transvers stirrups in the columns exhibited marginally smaller lateral strength (~10%) as compared to the RC specimen. This showed that SFRC could be used to reduce the transverse reinforcement in the beam-column joints of RC frame with strong-column and weak beam to achieve the nearly same lateral resistance and displacement ductility. The specimen SFRC-1.0%(2) sustained the displacement excursions corresponding to drift ratio of 6%, whereas other specimens failed at a drift ratio of 4.5%. Excessive reduction in the stiffness may lead to the higher displacement and the lower resistance to lateral loading resulting in the complete collapse of the specimen. Lateral stiffness of test specimens at any drift level was computed using the peak loads and displacements in both pull and push directions observed in the corresponding hysteretic loops in accordance with FEMA 356 (2000) guidelines. Fig. 10(b) shows the stiffness degradation of specimens at different drift levels. No significant difference in the stiffness degradation was noted in the response of test specimens. The degradation in lateral stiffness was nearly hyperbolic in nature for the test specimens.

Specimens with crossed inclined bars in the beam-column joints showed relatively inferior behavior under cyclic loading as compared to other specimens. These findings were contradictory to the results of past experimental studies (e.g., Tsonos *et al.* 1992, Tsonos 2004) in which the reinforcement detailing involving the crossed inclined bars showed the better cyclic performance. The reason for such a discrepancy may bemay be as follows: All beam longitudinal bars were bent in the diagonal configuration into the joint regions. This resulted in a reduction in the shear strength at the interfaces of beam-column joints where the longitudinal bars were bent. The use of some straight-through longitudinal bars of the beams would minimize the discontinuities and could have resulted better performance, which requires further investigations.

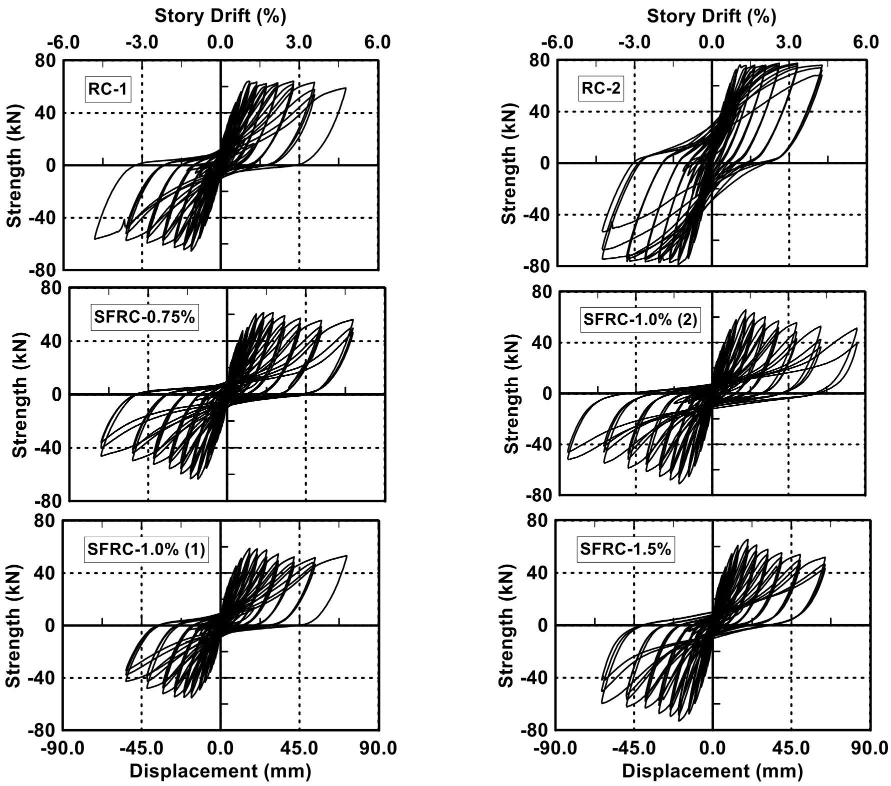

Fig. 9 Hysteretic response of test specimens

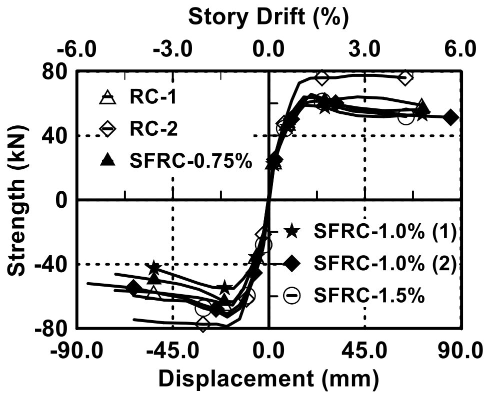

(a)

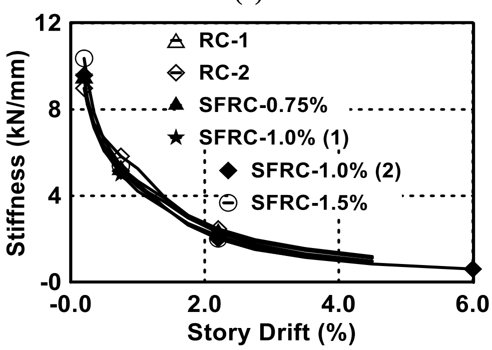

(b)

Fig. 10 Comparison of (a) backbone curves and (b) cyclic stiffness degradation of specimens

4.3 Energy dissipation and equivalent viscous damping

Energy dissipated by each specimen was computed from the enclosed area of the hysteretic loops. The variation of cumulative energy dissipated by the specimens at different drift ratios is shown in Fig. 11(a). At 0.5% drift level, SFRC-1.5% dissipated the maximum energy of 0.19 kNm followed by SFRC-1.0%(2) with 0.17 kNm and RC-2 with 0.14 kNm. Specimen RC-2 exhibited the maximum cumulative energy dissipation at 4.5% drift ratio, which was contributed primarily due to the high lateral load-resistance as discussed earlier. Except for the specimen RC-2, all the other specimens showed similar variation in the hysteretic energy dissipation capacity.

Equivalent viscous damping of the test specimens was computed using the following expression (FEMA 356 2000)

$$\beta_{eq} = \left(\frac{2}{\pi}\right)\left[E_{loop} \Big/ K_{eq}\left(D^{+} - D^{-}\right)^{2} \right] \tag{1}$$

Where, β_{eq} is the equivalent viscous damping, E_{loop} is the dissipated energy per hysteretic loop at a drift cycle, D is the recorded peak displacement, and K_{eq} is the effective stiffness. Fig. 11(b) shows the variation of the equivalent viscous damping with drift levels of specimens. Initial damping values of test specimens at the smaller drift cycles were found to be nearly same. However, the increased level of damage in the higher drift cycles resulted in the higher damping values. The maximum value of equivalent damping for the specimen RC-2 was computed as 61.5%, whereas all other specimens exhibited a maximum equivalent damping of nearly 42%.

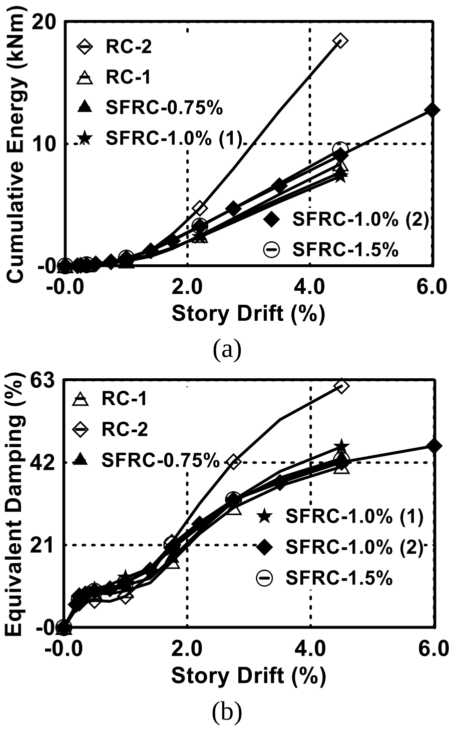

Fig. 11 (a) Cumulative energy dissipation and (c) Equivalent viscous damping of specimens

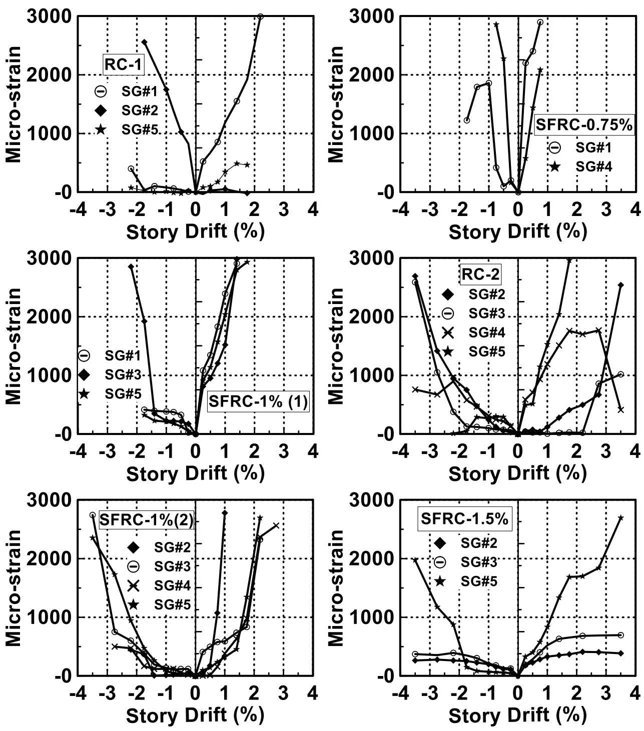

Fig. 12 State of strain in longitudinal reinforcing bars of beams

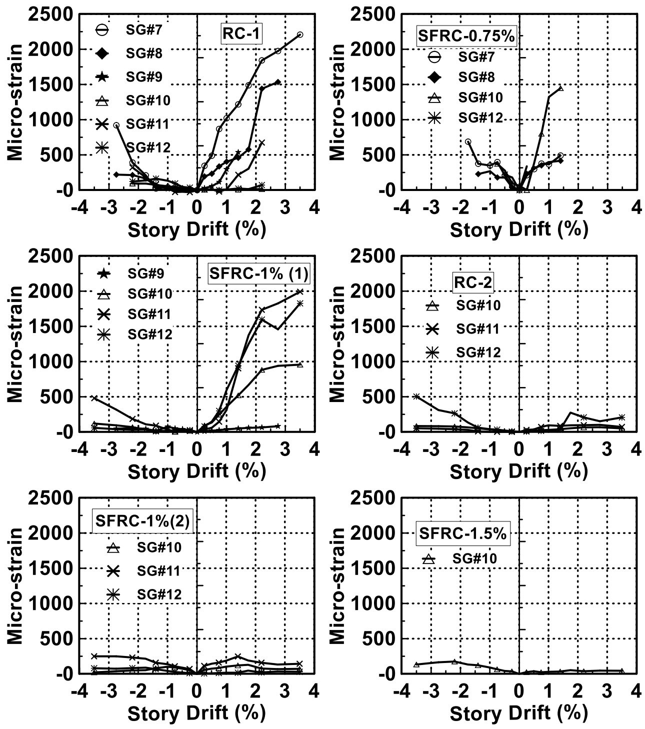

Fig. 13 State of strain in longitudinal reinforcing bars of columns

4.4 State of strain in reinforcement bars

The state of strain in the longitudinal reinforcing bars of beams and columns of specimens was monitored through uniaxial strain gauges attached to them near the beam-column joint regions (Fig. 6(a)). The mean values of peak strain noted in the repetitive cycles of a particular story drift were considered for the comparison purpose. Fig. 12 shows the variation of longitudinal strain in the reinforcement bars of beams. The magnitude of strain corresponding to yielding of steel bars was taken as 2000 micro-strain. Beam main reinforcing bars near to the beam-column joints of all specimens reached their yielding strain level. For the specimens RC-2, and SFRC-1%(2), yielding of longitudinal steel was delayed as compared to other three specimens. For the specimen SFRC-1.5%, most of the longitudinal bars did not yield till the end of the testing. The state of strain in the longitudinal reinforcements of columns is shown in Fig. 13. Since the flexural capacity of columns was higher than beams, the yielding of column bars was not noted in all specimens indicating their elastic behavior. Column bars of specimens RC-2, SFRC-1.0%(2), and SFRC-1.5% were subjected to very small magnitude of strain demand at all drift levels. Specimen RC-1 showed the maximum strain of 2.2% in the reinforcing bar.

4.5 Joint deformation

Displacements of beam-column joints in diagonal as well as horizontal/vertical directions were measured using LVDTs at different orientations as shown in Fig. 6(a). Two string-pots, namely, LVDTs-1 and 2 measured the relative diagonal displacements, whereas LVDTs-3, 4, 5 and 6 measured the relative horizontal displacements parallel to the beam at the beam-column joint. Fig. 14 shows the peak absolute values of diagonal and horizontal displacements at beam-column joints for of all specimens under lateral loading. The maximum diagonal displacement of 25.2 mm was observed in SFRC-1.0% (2) specimen, whereas the

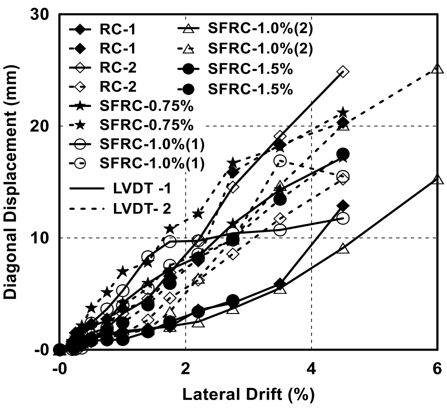

(a)

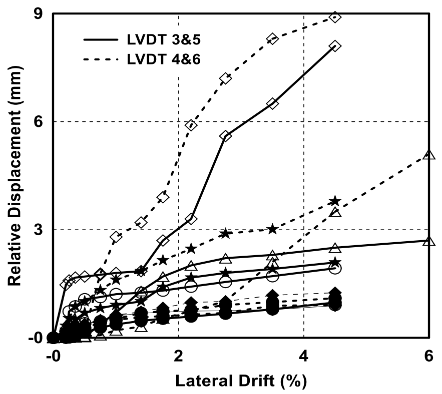

(b)

Fig. 14 Joint deformation: (a) diagonal displacement and (b) vertical displacement

corresponding values were varied in the range of 4.4-24.9 mm for other specimens. However, the relative horizontal displacement at various junctions of beam-column joints was noted in the range of 0.89 to 8.9 mm.

5. Analytical study

An analytical procedure is proposed to determine the load-resisting capacity of beam-column joints under lateral loading. The shear strength of beam-column joints is computed considering the contribution of concrete and reinforcing steel as discussed in the following sections.

5.1 Prediction of joint strength

Fig. 15 shows the typical tensile stress-displacement response of SFRC. SFRC has the better load-resisting capacity and ultimate displacement under the tensile loading. SFRC continues to resist the tensile stresses until the fibers are pulled out from the matrix (Lim *et al.* 1982). Accordingly, lateral load-resisting mechanism of SFRC beam-column joint involves the contribution of concrete, transverse reinforcement, and steel fiber (Jiuru *et al.* 1992). Fig. 16 shows the distribution of forces/stresses along with development of cracks in SFRC exterior beam-column joint under the action of lateral loading. The shear strength of SFRC beam-column joint can be expressed as follows:

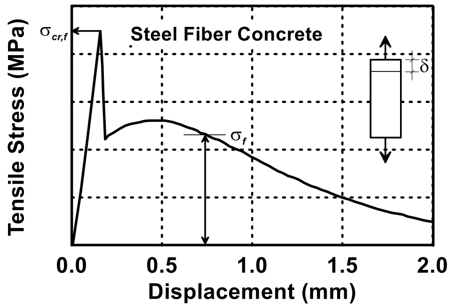

Fig. 15 Typical tensile stress *vs.* displacement curve of steel fiber concrete

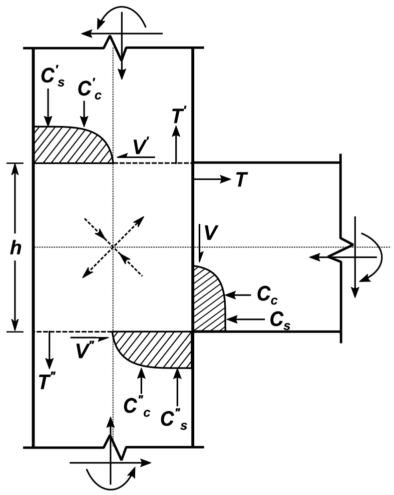

(a)

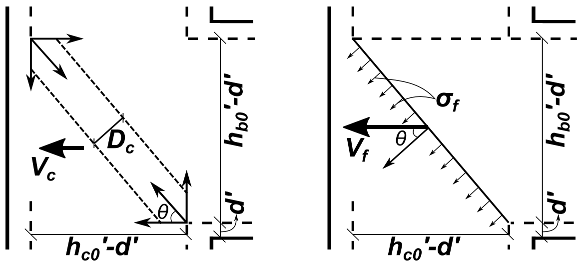

(b) (c)

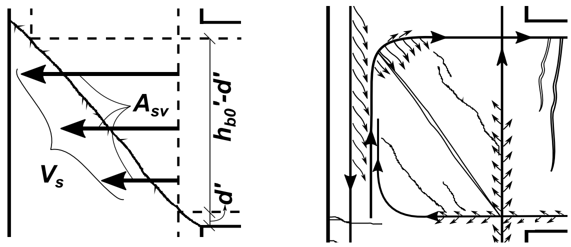

(d) (e)

Fig. 16 Exterior beam-column joint mechanism (a) typical stress distribution (b), (c), (d) shear resistance mechanism of SFRC joint and (e) crack propagation

$$V_j = V_c + V_f + V_s \qquad (2)$$

Where, V_j=ultimate shear strength of the SFRC joint, V_c= shear resisted by concrete which can be computed as follows (Jiuru *et al.* 1992).

$$V_c = 0.1\left(1+\frac{N}{b_c h_c f_{ck}}\right) b_j h_j h_c \quad (3)$$

Where, N is the axial compressive load of column, b_c and b_j are the width of column and the effective width of joint transverse to direction of shear respectively, h_c and h_j are the depth of column and the effective depth of joint parallel to the direction of shear respectively, and f_{ck} is the characteristics compressive strength of concrete.

Shear force carried by fibers (V_f) can be calculated as follows (Jiuru *et al.* 1992)

$$V_f = 2\frac{l_f}{d_f} v_f b_j h_j \quad (4)$$

Where, l_f is the length of fiber; d_f is the diameter of fiber; v_f if the steel fiber contents by volume of concrete. Finally, shear carried by transverse reinforcement can be calculated from the given equation

$$V_s = f_y \frac{A_{sv}}{s_v}\left(h_o - d'\right) \quad (5)$$

Where, f_y is the yield strength of shear reinforcement; A_{sv} is the area of shear reinforcement within distance s_v, h_o is the effective depth of beam; d' is the effective depth of cover concrete cover. Table 3 summarizes the calculated joint shear strength of beam-column joints using Eq. (2) and the comparison with the test results.

5.2 Prediction of joint strength

Lateral load-resisting capacity of test specimens was computed using classical method of beam analysis. The experimentally observed values were compared with those predicted using beam analysis. For beam analysis, lateral strength was computed using both flexural and shear capacity of members based on the concrete strength and reinforcement detailing. The smaller of these two computed values was considered as the lateral load-resisting capacity of the specimen. For RC members, the contribution of tensile strength of plain concrete was ignored in the lateral strength calculation. However, tensile strength of SFRC was considered in the classical method of beam analysis. Ultimate tensile strength of SFRC concrete (f_t) was calculated based on the following equation (Sahoo *et al.* 2016)

$$f_t = \alpha_o \alpha_b \sigma_f v_f \quad (6)$$

Where, α_o is the fiber orientation factor and is assumed as 0.41 (Oh 1992), α_b is the bond efficiency factor, which varies in the range of 1.0-1.2 based on fiber property (ACI-544.1R-96 2002). For end-hook fibers, this value could be taken as 1.2. σ_f and v_f are tensile strength of fiber and volume fraction of fiber, respectively.

Fig. 17 shows the assumed stress-strain distribution across a SFRC beam cross-section used in this study for the prediction of lateral capacity of test specimens. Linear variation of strain across the depth of section was assumed. Tensile stress distribution in SFRC beam gradually reduces towards the bottom after attaining a peak value near the neutral axis as shown in Fig. 17(c). For design purpose, the compressive stress block was assumed as the combination of rectangular and regular parabola and the tensile stress block in SFRC was assumed to be rectangular as shown in Fig. 17(d). The peak value of compressive stress in concrete was taken as $0.67f_{ck}$, where f_{ck} is the cube compressive strength.

The compressive force (C) on the section is the summation of compressive force from concrete (C_c) and compression zone longitudinal reinforcements (C_s). In the same way, the total tensile force (T) is the summation of tensile longitudinal reinforcements force (T_s) and tensile strength of SFRC (T_f). These compression and tension forces were calculated using the following equations

$$C_c = 0.54 f_{ck} b x_u \quad (7)$$

$$C_s = \left(f_{sc} - f_{cc}\right) A_{sc} \quad (8)$$

$$f_{sc} = f_y \quad \text{if } \varepsilon_{sc} = \varepsilon_y; \quad \text{else } f_{sc} = E\varepsilon_{sc} \quad (9)$$

$$f_{cc} = 0.67 f_{ck}\left[2\left(\frac{\varepsilon_c}{0.002}\right) - \left(\frac{\varepsilon_c}{0.002}\right)^2\right] \quad (10)$$

$$\varepsilon_{sc} = \frac{\varepsilon_{cu}\left(x_u - d'\right)}{x_u} \quad (11)$$

$$T_s = f_y A_{st} \quad (12)$$

$$T_f = f_t b(d - x_u)$$

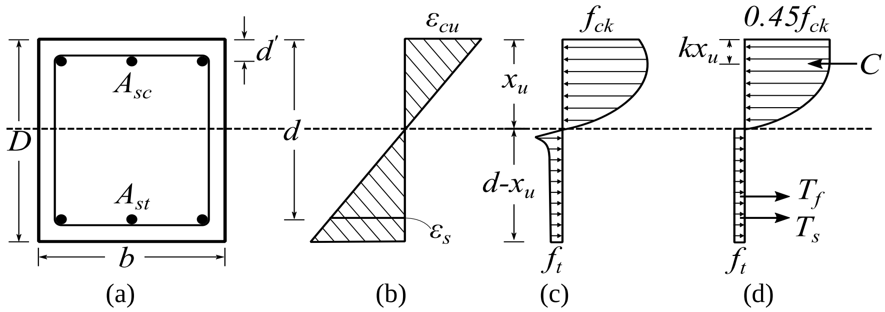

Fig. 17 Stress-strain distribution in SFRC beam section (a) Cross-section, (b) strain variation, (c) actual stress distribution and (d) design stress distribution

Table 3 Comparison of shear and flexural capacity of beam-column joint and columns and beams

Specimen	Moment capacity, kNm		Lateral strength based on flexure, kN		Lateral strength based on shear, kN		Pred. joint strength (V_j) kN	Obs. shear strength (V_{exp}), kN	Ratio $V_{exp}/V'_{b,beam}$	Ratio V_{exp} / V_j
	Column (M_{pc})	Beam (M_{pb})	Column ($V'_{b,col}$)	Beam ($V'_{b,beam}$)	Column ($V'_{c,col}$)	Beam ($V'_{c,beam}$)				
RC-1	65.6	61.2	39.7	55.2	167.9	167.9	174.7	65.4	1.18	0.37
SFRC-0.75%	74.9	71.5	45.3	64.4	195.2	206.5	179.6	63.4	0.98	0.35
SFRC-1.0%(1)	78.0	75.3	47.2	67.9	207.3	220.4	181.3	59.0	0.87	0.32
RC-2	102.7	73.1	62.1	65.9	196.9	188.4	194.6	82.6	1.25	0.42
SFRC-1.0%(2)	123.0	88.7	74.4	80.0	249.8	234.9	191.6	70.9	0.89	0.37
SFRC-1.5%	133.1	97.3	80.5	87.7	266.0	249.0	194.7	72.8	0.83	0.38

Flexural capacity of a member was calculated as follows

$$M_u = C_c(x_u - kx_u) + C_s d' + T_s(d - x_u) + 0.5T_f(d - x_u) \quad (14)$$

Where, k is a factor to quantify the distance of resultant compressive force from the extreme compression top fiber. The value of T_f in the above equations was zero for RC members. The lateral force required to achieve the flexural capacity of the member was computed as follows

$$V'_b = M_u / a \quad (15)$$

Where, a is the shear span. Shear-resisting capacity of a member was calculated as the sum of the contribution of concrete and the shear stirrups as follows

$$V'_c = \tau_{sf} bd + f_y A_{sv} d / s_v \quad (16)$$

Where, A_{sv} and s_v are area of shear stirrups and spacing of stirrups; τ_{sf} is shear stress of concrete. For SFRC, τ_{sf} was estimated using the following expression (Kwak *et al.* 2002).

$$\tau_{sf} = 3 f_{sf}^{\,2/3} \left(\rho \, d/a\right)^{1/3} \quad (17)$$

Where, f_{sf} = split cylinder tensile strength and ρ = flexural steel reinforcement ratio.

Table 3 shows the predicted flexural and shear capacities with the observed joint shear strength of all test specimens. The ratio of flexural capacity of columns to those of beams for each specimen was relatively higher than those adopted in the practice. In each case, shear capacity of beam was smaller than the flexural capacity. In addition, beam-column joint shear capacity was much higher than the normal shear of beam and column. As result, failure of all specimens was observed near the beam-column joint. Moreover, the predicted lateral strengths for RC specimens were found to be higher by about 20% as compared to the test results. On the other hand, the predicted lateral strengths of SFRC specimens reasonably matched well with the experimental values.

6. Conclusions

An experimental investigation was conducted on six beam-column test specimens under constant axial load and lateral cyclic loading. Steel fiber reinforce concrete (SFRC) was used in the beam-column joints with fiber content varying in the range of 0.75-1.5%. Two different detailing schemes were adopted at the beam-column joint regions. The following conclusions can be drawn from the present study:

• Test specimens with beam longitudinal bars placed diagonally in the beam-column joints exhibited the interfacial shear cracks irrespective of the quantity of transverse stirrups in the joints. RC specimen with straight beam longitudinal bars exhibited flexural plastic hinge away from the joint regions.

• Test specimens with steel fiber-reinforced concrete (SFRC) with fiber content in the range of 0.75-1.5% in the beam-column joints resulted in the same displacement ductility and mode of failure along with marginally smaller lateral strength as the control RC specimen. All test specimens exhibited the similar energy dissipation, equivalent viscous damping, and stiffness degradation at all lateral drift levels.

• The use of SFRC in the beam-column joint regions could reduce the requirement of transverse shear stirrups in the beam-column joints for specimens designed with strong column and weak-beam concept. SFRC specimens with reduced transverse reinforcement showed the stable hysteretic response, excellent ductility, and the better energy dissipation

• The increase in fiber content increased the number of minor cracks in the critical regions due to the fiber bridging action. Considering the higher fiber content has an adverse effect on workability of fresh concrete, the use of fiber content of 0.5-1.0% in the SFRC beam-column joints is recommended.

• The use of all beam longitudinal bars in crossed inclined configuration in the joints resulted in the reduction in the shear strength at the beam-column interfaces. Further investigation is required to study the cyclic behavior of SFRC beam-column joints using a combination of straight-through and bent bars of beam longitudinal reinforcement.

Acknowledgments

The research described in this paper was financially supported by the Ministry of Human Resource Development, India. Authors are thankful to the laboratory staff members of Heavy Structures Laboratory, IIT Delhi for their help and support during the experiment.

References

Abbas, A.A., Syed, Mohsin, S.M. and Cotsovos, D.M. (2014), “Seismic response of steel fibre reinforced concrete beam-column joints”, *Eng. Struct.*, **59**, 261-283. https://doi.org/10.1016/j.engstruct.2013.10.046.

ACI-544.1R-96 (2002), Design Considerations for Steel Fiber Reinforced Concrete, American Concrete Institute, Farmington Hills, Michigan, USA.

ACI 374.1-05 (2006), Acceptance Criteria for Moment Frames based on Structural Testing and Commentary- An ACI Standard, American Concrete Institute, Farmington Hills, MI, USA.

Aoude, H., Belghiti, M., Cook, W.D. and Mitchell, D. (2012), “Response of steel fiber-reinforced concrete beams with and without stirrups”, *ACI Struct J.*, **109**(3), 359-368.

ASCE 41-13 (2013), Seismic Evaluation and Retrofit of Existing Buildings, American Society of Civil Engineers, Reston, Virginia, USA.

ASTM C1609/C1609M (2006), Standard Test Method for Flexural Performance of Fiber-reinforced Concrete, American Society for Testing and Materials, West Conshohocken, PA, USA.

Barbhuiya, S. and Choudhury, A.M. (2015), “A study on the size effect of RC beam-column connections under cyclic loading”, *Eng. Struct.*, **95**, 1-7. https://doi.org/10.1016/j.engstruct.2015.03.052.

Bayasi, Z. and Gebman, M. (2002), “Reduction of lateral reinforcement in seismic beam-column connection via application of steel fibers”, *ACI Struct. J.*, **99**(78), 772-780. https://doi.org/10.1016/j.engstruct.2015.03.052.

Chutarat, N. and Aboutaha, R.S. (2003), “Cyclic response of exterior reinforced concrete beam-column joints reinforced with headed bars-Experimental investigation”, *ACI Struct. J.*, **100**(2), 259-264.

Dinh, H.H., Parra-Montesinos, G.J. and Wight, J.K. (2010), “Shear strength of steel fiber reinforced concrete beams without stirrup reinforcement”, *ACI Struct. J.*, **107**(5), 597-606.

Eurocode 8 (2004), Design of Structures for Earthquake Resistance, British Standards Institution, London, UK.

FEMA 356 (2000), Prestandard and Commentary for the Seismic Rehabilitation of Buildings, Applied Technology Council, Washington, DC, USA.

Filiatrault, A., Ladicani, K. and Massicotte, B. (1994), “Seismic performance of code-designed fiber-reinforced concrete joints”, *ACI Struct. J.*, **91**(54), 564-571.

Gefken, P.R. and Ramey, M.R. (1989), “Increased joint hoop spacing in type 2 seismic joints using fiber reinforced concrete”, *ACI Struct. J.*, **56**(19), 168-172.

Harajli, M.H., Hout, M. and Jalkh, W. (1995), “Local bond stress-slip behavior of reinforcing bars embedded in plain and fiber concrete”, *ACI Mater J.*, **92**(4), 343-354.

IS:10262 (2009), Concrete Mix Proportioning-Guidelines, Bureau of Indian Standards, New Delhi, India.

IS:1893 (2016), Criteria for Earthquake Resistant Design of Structures, Bureau of Indian Standards, New Delhi, India.

IS:456 (2000), Plain and Reinforced Concrete - Code of Practice, Bureau of Indian Standards, New Delhi, India.

IS:516-1959 (2004), Methods of Tests for Strength of Concrete, Bureau of Indian Standards, New Delhi, India.

IS:5816 (1999), Splitting Tensile Strength of Concrete, Bureau of Indian Standards, New Delhi, India.

Jiuru, T., Chaobin, H., Kaijian, Y. and Yongcheng, Y. (1992), “Seismic behavior and shear strength of framed joint using steel-fiber reinforced concrete”, *ASCE J. Struct. Eng.*, **118**(2), 341-358. https://doi.org/10.1061/(ASCE)0733-9445(1992)118:2(341).

Karayannis, C.G. and Golias, E. (2018), “Full scale tests of RC joints with minor to moderate seismic damage repaired using C-FRP sheets”, *Earthq. Struct.*, **15**(6), 617-627. https://doi.org/10.12989/eas.2018.15.6.617.

Kheni, D., Scott, R.H., Deb, S.K. and Dutta, A. (2015), “Ductility enhancement in beam-column connections using hybrid fiber-reinforced concrete”, *ACI Struct. J.*, **112**(2), 167-178.

Kwak, Y.K., Eberhard, M.O., Kim, W.S. and Kim, J. (2002), “Shear strength of steel fiber-reinforced concrete beams without stirrups”, *ACI Struct J.*, **99**(4), 530-538.

Lee, H.H. (2007), “Shear strength and behavior of steel fiber reinforced concrete columns under seismic loading”, *Eng. Struct.*, **29**(7), 1253-1262. https://doi.org/10.1016/j.engstruct.2006.08.016.

Li, B., Lam, E.S., Cheng, Y., Wu, B. and Wang, Y. (2015), “Strengthening of non-seismically designed beam-column joints by ferrocement jackets with chamfers”, *Earthq. Struct.*, **8**(5), 1017-1038. https://doi.org/10.12989/eas.2015.8.5.1017.

Lim, T.Y., Paramasivam, P. and Lee, S.L. (1987), “Analytical model for tensile behavior of steel-fiber concrete”, *ACI Mater. J.*, **84**(4), 286-298.

Liu, C. (2006), “Seismic behaviour of beam-column joint subassemblies reinforced with steel fibres”, Master’s Thesis, Department of Civil Engineering, University of Canterbury, Christchurch, NZ.

Lu, X., Urukap, T.H., Li, S. and Lin, F. (2012), “Seismic behavior of interior RC beam-column joints with additional bars under cyclic loading”, *Earthq. Struct.*, **3**(1), 37-57. http://dx.doi.org/10.12989/eas.2012.3.1.037.

Murty, C.V.R., Rai, D.C., Bajpai, K.K. and Jain, S.K. (2004), “Effectiveness of reinforcement details in exterior reinforced concrete beam-column joints for earthquake resistance”, *ACI Struct. J.*, **101**(2), 149-156.

Oh, H. (1992), “Flexural analysis of reinforced concrete beams containing steel fibers”, *ASCE J. Struct. Eng.*, **118**(10), 2821-2835. https://doi.org/10.1061/(ASCE)0733-9445(1992)118:10(2821).

Oinam, R.M., Sahoo, D.R. and Sindhu, R. (2014), “Cyclic response of non-ductile RC frame with steel fibers at beam-column joints and plastic hinge regions”, *J. Earthq. Eng.*, **18**(6), 908-928. https://doi.org/10.1080/13632469.2014.916239.

Park, R. and Paulay, T. (1975), *Reinforced Concrete Structures*, John Wiley and Sons, NY, USA.

Park, S. and Mosalam, K.M. (2012), “Parameters for shear strength prediction of exterior beam-column joints without transverse reinforcement”, *Eng. Struct.*, **36**, 198-209. https://doi.org/10.1016/j.engstruct.2011.11.017.

Paulay, T. and Priestley, M. (1992), *Seismic Design of Reinforced Concrete and Masonry Buildings*, John Wiley and Sons, Inc., NY, USA.

Paulay, T., Park, R. and Priestley, M.J.N. (1978), “Reinforced concrete beam-column joints under seismic actions”, *ACI Struct. J.*, **75**(11), 585-593.

Rajagopal, S., Prabavathy, S. and Kang, T.H.-K. (2014), “Seismic behavior evaluation of exterior beam-column joints with headed or hooked bars using nonlinear finite element analysis”, *Earthq. Struct.*, **7**(5), 861-875. https://doi.org/10.12989/eas.2014.7.5.861.

Sahoo, D.R. and Kumar, N. (2015), “Monotonic behavior of large-scale SFRC beams without stirrups”, *Eng. Struct.*, **92**, 46-54. https://doi.org/10.1016/j.engstruct.2015.03.014.

Sahoo, D.R. and Sharma, A. (2014), "Effect of steel fiber content on behavior of concrete beams with and without stirrups", *ACI Struct. J.*, **111**(5), 1157-1166

Sahoo, D.R., Bhagat, S. and Reddy, T.C.V. (2016), "Experimental study on shear-span to effective-depth ratio of steel fiber reinforced concrete T-beams", *Mater. Struct.*, **49**(9), 3815-3830. https://doi.org/10.1617/s11527-015-0756-6.

Sahoo, D.R., Solanki, A. and Kumar, A. (2015), "Influence of steel and polypropylene fibers on flexural behavior of RC beams", *ASCE J. Mater. Civil Eng.*, **27**(8), 04014232. https://doi.org/10.1061/(ASCE)MT.1943-5533.0001193.

Tsonos, A.G. (1992), "Seismic resistance of Type 2 exterior beam-column joints reinforced with inclined bars", *ACI Struct. J.*, **89**(1), 3-12.

Tsonos, A.G. (2004), "Improvement of the earthquake resistance of R/C beam-column joints under the influence of P-Δ effect and axial force variations using inclined bars", *Struct. Eng. Mech.*, **18**(4), 389-410. https://doi.org/10.12989/sem.2004.18.4.389.

Tsonos, A.G. (2007), "Cyclic load behaviour of reinforced concrete beam-column subassemblages of modern structures", *ACI Struct. J.*, **194**(4), 468-478. https://doi.org/10.2495/ERES050421

Tsonos, A.G. (2014), "A new method for earthquake strengthening of old R/C structures without the use of conventional reinforcement", *Struct. Eng. Mech.*, **52**(2), 391-403. : http://dx.doi.org/10.12989/sem.2014.52.2.391.

Yang, Y., Chen, Y., Chen, Z., Wang, N. and Yu, Y. (2018), "Experimental study on seismic behavior of RC beam-column joints retrofitted using prestressed steel strips", *Earthq. Struct.*, **15**(5), 499-511. https://doi.org/10.12989/eas.2018.15.5.499.

AT

Symbols

A_{sc}	Area of compression reinforcement
A_{sv}	Area of shear stirrups
C_c	Compressive force from concrete
D^+, D^-	Recorded peak displacement
K_{eq}	Effective stiffness
N	Axial compressive load of column
T_s	Tensile force from tensile longitudinal reinforcements
V_j	Ultimate shear strength of the SFRC joint
V_f	Shear carried by fibers
V'_b	Lateral force which required to reach the ultimate flexural capacity
a & a_e	Shear span in beam and column
b_c	Effective width of column
d	Effective depth of beam/column section
d'	Effective cover
f_{ck}	Cube compressive strength
f_{sf}	Split cylinder tensile strength
f_y	Yield strength of reinforcement bars
h_j	Effective depth of joint parallel to direction of shear
l_d	Development length
s_v	Spacing of stirrups
v_f	Steel fiber contents
α_b	Bond efficiency factor
ε_c	Strain in concrete
ε_{sc}	Strain in compression reinforcement
ρ	Flexural steel reinforcement ratio
τ_{sf}	Shear stress of concrete
A_{st}	Area of tensile reinforcement
C	Total compressive force on the section
C_s	Compression force in reinforcements
E_{loop}	Dissipated energy per hysteretic loop
M_u	Ultimate flexural capacity of beam section
T	Total tensile force on the section
T_f	Tensile strength of SFRC
V_c	Shear carried by concrete
V_s	Shear carried by transverse reinforcement
V'_c	Shear resisting capacity of member section
b	Width of beam/column section
b_j	Effective width of joint
d_f	Diameter of fiber
f_{cc}	Stress in concrete which is correspond to f_{sc}
f_{sc}	Stress compression reinforcement bars
f_t	Ultimate tensile strength of SFRC concrete
h_c	Effective depth of column
k	Factor to quantify the distance of resultant compressive force
l_f	Length of fiber
x_u	Depth of the neutral axis
α_o	Fiber orientation factor
β_{eq}	Equivalent viscous damping
ε_{cu}	Ultimate strain in concrete
ε_y	Yield strain in concrete
σ_f	Tensile strength of fiber